OXFORD

Human Molecular Genetics, 2023, Vol. 32, 13, 2177–2191
https://doi.org/10.1093/hmg/ddad054
Advance access publication date 3 April 2023
Original Article

A humanized yeast model reveals dominant-negative properties of neuropathy-associated alanyl-tRNA synthetase mutations

Rebecca Meyer-Schuman[1], Sheila Marte[1], Tyler J. Smith[2], Shawna M.E. Feely[3], Marina Kennerson[4,5,6], Garth Nicholson[4,5,6], Mike E. Shy[3], Kristin S. Koutmou[2] and Anthony Antonellis[1,7,*]

[1]Department of Human Genetics, University of Michigan Medical School, Ann Arbor, MI 48109, USA
[2]Department of Chemistry, University of Michigan, Ann Arbor, MI 48109, USA
[3]Department of Neurology, Carver College of Medicine, University of Iowa, Iowa City, IA 52242, USA
[4]Northcott Neuroscience Laboratory, ANZAC Research Institute, Sydney, NSW 2139, Australia
[5]Sydney Medical School, University of Sydney, Sydney, NSW 2050, Australia
[6]Molecular Medicine Laboratory, Concord General Repatriation Hospital, Sydney, NSW 2139, Australia
[7]Department of Neurology, University of Michigan Medical School, Ann Arbor, MI 48109, USA

*To whom correspondence should be addressed. Tel: +1 7346474058; Fax: +1 7347633784; Email: antonell@umich.edu

Abstract

Aminoacyl-tRNA synthetases (ARSs) are essential enzymes that ligate tRNA molecules to cognate amino acids. Heterozygosity for missense variants or small in-frame deletions in six ARS genes causes dominant axonal peripheral neuropathy. These pathogenic variants reduce enzyme activity without significantly decreasing protein levels and reside in genes encoding homo-dimeric enzymes. These observations raise the possibility that neuropathy-associated ARS variants exert a dominant-negative effect, reducing overall ARS activity below a threshold required for peripheral nerve function. To test such variants for dominant-negative properties, we developed a humanized yeast assay to co-express pathogenic human alanyl-tRNA synthetase (*AARS1*) mutations with wild-type human *AARS1*. We show that multiple loss-of-function *AARS1* mutations impair yeast growth through an interaction with wild-type *AARS1*, but that reducing this interaction rescues yeast growth. This suggests that neuropathy-associated *AARS1* variants exert a dominant-negative effect, which supports a common, loss-of-function mechanism for ARS-mediated dominant peripheral neuropathy.

Introduction

Hereditary peripheral neuropathies are a group of phenotypically and genetically heterogeneous diseases that are characterized by decreased sensory and/or motor axon function in the distal extremities. This leads to sensory loss and muscle atrophy, which often begins in the feet and lower legs, and may progress to include the hands and forearms of the upper extremities (1,2). The most common type of inherited peripheral neuropathy is Charcot-Marie-Tooth (CMT) disease, which is estimated to affect between 1 in 1200 and 1 in 2500 individuals (3,4).

In total, mutations in over 100 genes have been associated with CMT disease or related inherited peripheral neuropathies (5). Among these are the aminoacyl-tRNA synthetase (ARS) genes, a 37-member gene family that encodes ubiquitously expressed, essential enzymes. ARSs act as either monomers or oligomers to ligate tRNA molecules to cognate amino acids, forming a critical substrate for protein translation (6). Variants in six aminoacyl-tRNA synthetases have been linked to dominant peripheral neuropathies: alanyl-(*AARS1*) (7) histidyl-(*HARS1*) (8) glycyl-(*GARS1*) (9), seryl-(*SARS1*) (10), tryptophanyl-(*WARS1*) (11) and tyrosyl-(*YARS1*) tRNA synthetase (12). Although methionyl-tRNA synthetase variants have also been identified in patients with CMT disease (13,14), the genetic evidence for the pathogenicity of these alleles is still incomplete. It remains to be seen how many additional ARSs will be implicated in dominant peripheral neuropathy. Further defining the locus and allelic heterogeneity of ARS-related neuropathy will be critical for patient diagnosis and defining disease mechanisms.

ARS activity is essential for cellular function. Indeed, bi-allelic ARS variants that reduce enzyme function cause early-onset recessive disorders that affect multiple tissues (15,16). In many cases, the constellation of recessive phenotypes includes peripheral neuropathy (17–19), demonstrating that peripheral nerves are indeed sensitive to a reduction of ARS function. However, this reduction must be more than 50%, because heterozygosity for a null ARS allele is not sufficient to cause a penetrant neuropathic phenotype; mono-allelic null alleles are not found in CMT patient populations but are found in unaffected individuals. Additionally, mice that are heterozygous for a *Gars1* null allele do not develop peripheral neuropathy, whereas those carrying loss-of-function missense and in-frame deletion alleles do develop this phenotype (20–22). Based on these observations, haploinsufficiency is an unlikely disease mechanism for ARS-associated dominant neuropathy.

The pathogenic ARS variants linked to dominant peripheral neuropathy are exclusively missense mutations or small in-frame deletions (23). As noted above, ARS frameshift alleles and premature stop codons have not been linked to dominant CMT disease,

Received: January 4, 2023. **Revised:** March 29, 2023. **Accepted:** March 30, 2023

which indicates that an expressed mutant protein is required for pathogenicity. It is currently unknown if the dozens of identified pathogenic variants across the six implicated ARS genes (11,22–29) exert a similar effect on a shared pathway, or if there are unique pathogenic mechanisms for each locus. One proposed mechanism is a neomorphic gain-of-function effect, in which mutations expose novel protein interfaces that facilitate aberrant protein–protein interactions, leading to the dysregulation of pathways important for neurons (30–35). However, it is unlikely that the dozens of different alleles across all six ARS loci give rise to an identical gain-of-function effect via aberrant interactions. Rather, any common mechanism would likely be related to the shared canonical function of charging tRNA in the cytoplasm and axoplasm of peripheral neurons.

One notable commonality is that all six enzymes function as homodimers. This raises the possibility of a dominant-negative mechanism, in which decreased function of the mutant subunit reduces the function of the wild-type subunit in the dimer; this would lower the overall ARS activity in the cell below 50%. This mechanism is supported by an abundance of data showing that the majority of neuropathy-associated ARS variants reduce gene function (10,11,22–24,26–28). Additionally, pathogenic variants do not decrease protein levels (21,22,36) nor do they abolish dimerization (10–12,28,37,38). It has also been shown that pathogenic ARS variants impair protein synthesis in affected neurons. Expressing neuropathy-associated ARS alleles causes decreased global protein translation *in vitro* (11,37,39) and *in vivo* (40,41), increases eIF2-alpha phosphorylation (37,39,41) and activates the integrated stress response (37,39,41). Importantly, these phenotypes can be recapitulated *in vitro* by chemical inhibition of the affected ARS enzyme (37), which directly links these phenotypes to impaired enzyme function. These effects have been further defined at the molecular level for several *GARS1* mutations, which impair the release of tRNA from the enzyme (39,42). Cumulatively, these studies demonstrate that pathogenic ARS mutations reduce the enzyme's ability to bind, charge, or release tRNA, impacting protein translation and contributing to the pathogenic mechanism. Considering the evidence against haploinsufficiency, it is possible that these impairments are exacerbated by pathogenic ARS alleles that interfere with the function of the wild-type allele in a dominant-negative fashion. In support of this, previous studies in yeast have shown that cells co-expressing both wild-type and mutant neuropathy-associated tyrosyl-tRNA synthetase variants show impaired growth, compared to cells expressing only wild-type tyrosyl-tRNA synthetase (12). However, it remains unclear if these phenotypes are due to a dominant-negative effect or an unrelated toxic effect of the mutant allele. Addressing this question will attempt to identify a unifying mechanism of disease for all six implicated dimeric ARS enzymes. Furthermore, developing an approach to systematically assess ARS variants for a dominant-negative effect will provide a relevant framework to assess the pathogenicity of newly identified ARS variants in patients with dominant CMT disease.

Here, we report a yeast model system to test human pathogenic ARS variants for dominant-negative properties. Yeast is a tractable model organism that can be adapted to study highly conserved human genes, along with mutations in these genes that affect gene function, impact conserved cellular pathways and ultimately reduce yeast fitness (43,44). This is particularly relevant for conserved pathways implicated in ARS pathology including protein translation and the integrated stress response (37,39,41,42). As recent studies in HEK293T cells have demonstrated (39), studying the effect of neuropathy-associated ARS alleles in non-neuronal systems can yield important and informative insight into disease mechanisms. To this end, we developed a yeast model to test human *AARS1* variants for dominant-negative properties. We focused on well-characterized alleles in the anti-codon binding domain (R329H) (7,25,45,46) and the amino acid activation domain (G102R) (47). We found that R329H and G102R, as well as three additional *AARS1* variants (R326W, R329S and R329C), have a dominant, repressive effect on yeast cell growth when co-expressed with wild-type human *AARS1*. We then engineered a dimer-disrupting variant in the C-terminal domain and modeled it in *cis* with pathogenic *AARS1* variants. These double-mutants rescued the impaired yeast growth, demonstrating that the dominant effect of mutant *AARS1* is dependent on dimerization with wild-type *AARS1* and that neuropathy-associated *AARS1* variants can be classified as dominant-negative (or antimorphic) alleles.

Results

Pathogenic *AARS1* alleles repress yeast cell growth in the presence of wild-type *AARS1*

Baker's yeast (*Saccharomyces cerevisiae*) is an effective model to study the functional consequences of pathogenic ARS alleles in a living cell (23). To investigate dominant-negative properties of neuropathy-associated *AARS1* variants, we developed an assay to test the effects of co-expressing human wild-type *AARS1* and human mutant *AARS1* on yeast viability, using the ptetO7-*ALA1* strain. In this strain, the yeast *AARS1* ortholog, *ALA1*, is placed under the control of a doxycycline-repressible promoter (48). We transformed this strain with (1) a low-copy, centromere-bearing vector (p413) (49) containing a wild-type *AARS1* allele; and (2) a high-copy number vector (i.e. bearing a 2-μm origin of replication) with a galactose-inducible promoter (pAG425) (50) directing high levels of expression of either wild-type or mutant *AARS1* alleles (Supplementary Material, Fig. S1A and B). To test mutant *AARS1* alleles for a dominant effect on yeast cell growth, yeast cells were grown in the presence of galactose (to express wild-type or mutant *AARS1* from the pAG425 vector) and doxycycline (to repress endogenous *ALA1*); in this system, wild-type *AARS1* is constitutively expressed from p413. Subsequent yeast growth was then solely dependent on the two forms of human *AARS1*: one wild-type (from p413) and one wild-type or mutant (from pAG425).

To evaluate neuropathy-associated *AARS1* variants for a dominant-negative effect, we focused on two well-characterized pathogenic *AARS1* variants, R329H and G102R. R329H is a recurrent mutation in the tRNA recognition domain that has been identified in 10 families with dominant, axonal CMT (7,25,45,46,51). It affects a highly conserved residue and significantly impairs *AARS1* enzymatic function when assessed via *in vitro* aminoacylation assays under Michaelis–Menten conditions (45). The G102R *AARS1* variant affects a highly conserved residue in the activation domain of *AARS1* and was found in a single pedigree with dominant myeloneuropathy (47). Both G102R and R329H have been modeled in the yeast ortholog *ALA1*, and were unable to support yeast growth, indicating a loss-of-function effect *in vivo* (45,47). To distinguish the dominant-negative properties of these variants from a strictly loss-of-function effect, we generated a premature stop codon, G757* (Supplementary Material, Fig. S1A), which does not generate detectable levels of *AARS1* protein (Supplementary Material, Fig. S1B). Therefore, this variant is expected to be a loss-of-function allele that does not exert dominant-negative effects. This variant is a more precise negative

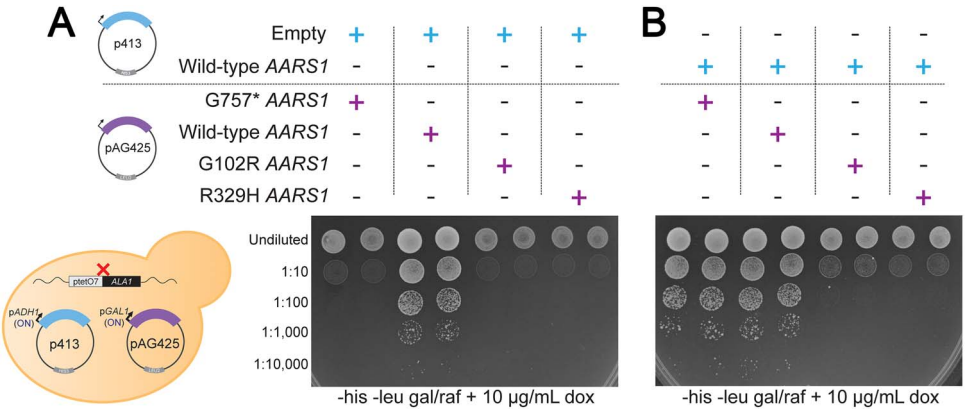

Figure 1. G102R and R329H *AARS1* are loss-of-function alleles that repress yeast cell growth in the presence of wild-type *AARS1*. (**A**) Yeast harboring an endogenous doxycycline-repressible *ALA1* locus were transformed with a p413 vector with no insert and a pAG425 vector to express either wild-type or mutant human *AARS1*. Cultures were plated undiluted or diluted on media lacking histidine and leucine, and containing galactose/raffinose and doxycycline. (**B**) Similar experiment as shown in panel A; here, yeast were first transformed with a p413 vector expressing wild-type human *AARS1*. For both panels, the vectors present in each experiment are indicated across the top, the dilution of the spotted yeast cultured is indicated on the left side of the image, and the media conditions are indicated across the bottom of the image (his = histidine; leu = leucine; gal = galactose; raf = raffinose; dox = doxycycline). Representative images are shown from thirteen (for G102R) or sixteen (for R329H) biological replicates. A cartoon on the bottom left illustrates the experimental conditions for all samples.

control than an empty vector because it includes the *AARS1* coding sequence. Yeast transformed with the G757* allele must replicate a nearly identical DNA sequence, and express a nearly identical mRNA sequence, as yeast transformed with the G102R or R329H alleles.

To confirm that R329H and G102R human *AARS1* are loss-of-function alleles in a yeast complementation assay, ptetO7-*ALA1* yeast was first transformed with a p413 vector without an *AARS1* coding sequence ('Empty' in the relevant figures), then with pAG425 expressing either wild-type or mutant human *AARS1*. When these strains were plated on media containing glucose, there were no observable growth defects (Supplementary Material, Fig. S2A). When these strains were plated on media containing galactose and doxycycline, the yeast expressing G757* did not display any visible growth (Fig. 1A), indicating that yeast cannot grow without *ALA1* expression (i.e. without functional *AARS1* protein). Transformation with wild-type *AARS1* lead to robust yeast growth, confirming that wild-type human *AARS1* can complement the loss of yeast *ALA1*. Neither G102R nor R329H *AARS1* supported yeast growth (Fig. 1A), confirming previous reports that these are loss-of-function alleles *in vivo* (45,47).

To determine if mutant *AARS1* alleles can repress the function of wild-type *AARS1*, ptetO7-*ALA1* yeast cells were transformed with wild-type *AARS1* on the low-copy p413 vector, then with wild-type or mutant *AARS1* on the high-copy pAG425 vector. Transformed strains spotted on glucose media displayed no observable growth defects (Supplementary Material, Fig. S2B). These strains were then spotted on galactose (to induce expression from the pAG425 vector) and doxycycline (to repress *ALA1* expression). Co-expression of wild-type and G757* *AARS1* supported robust growth, as did co-expression of the two wild-type *AARS1* plasmids (Fig. 1B). These data indicate that the G757* null allele has no negative impact on yeast cell growth and, similarly, that expressing two copies of wild-type *AARS1* does not repress yeast growth. In contrast, co-expression of wild-type *AARS1* with either G102R or R329H *AARS1* caused significantly reduced yeast growth (Fig. 1B). These data demonstrate that the two pathogenic, neuropathy-associated alleles are not only loss-of-function alleles but that they are also detrimental to yeast cell growth in the presence of wild-type *AARS1*. These observations are consistent with mutant *AARS1* interfering with the function of the wild-type *AARS1* protein. Importantly, the mutation-associated growth deficit is partially rescued by restoring *ALA1* expression (Supplementary Material, Fig. S3A), which increases growth 23-fold for yeast expressing G102R and 11-fold for yeast expressing R329H (Supplementary Material, Fig. S3B). These data suggest that the dominant growth deficit caused by R329H and G102R *AARS1* is due to reduced alanine-tRNA charging. Interestingly, *ALA1* only partially rescues the growth deficit associated with R329H. This may be related to our observation that human R329H *AARS1* interacts with ALA1 (Supplementary Material, Fig. S4B), suggesting that human R329H *AARS1* has a dominant-negative effect on wild-type yeast ALA1.

Pathogenic *AARS1* variants do not ablate dimerization

The data presented above demonstrate that the pathogenic, loss-of-function *AARS1* variants G102R and R329H *AARS1* dominantly repress yeast cell growth in the presence of wild-type *AARS1*, consistent with a dominant-negative effect. However, the data do not rule out some other form of gain-of-function toxicity unrelated to the *AARS1* function. To directly test for a dominant-negative effect, we first confirmed that mutant *AARS1* dimerizes with wild-type *AARS1*. As ultracentrifugation analyses have demonstrated that isolated mutant ARS proteins retain the dimerization properties of wild-type ARS proteins (28,37,38), we hypothesized that mutant *AARS1* also retained its ability to dimerize with wild-type *AARS1*. To directly test this, HEK293T cells were transfected with a vector expressing wild-type human *AARS1* with an in-frame C-terminal 3xFLAG tag and with a vector expressing mutant AARS1 (G102R or R329H) with an in-frame C-terminal 6xHis tag (Fig. 2A). After growth for 48 h, cells were lysed and *AARS1*-6xHis was immunoprecipitated. Co-immunoprecipitated proteins were subjected to western blot analysis with an anti-FLAG antibody to detect *AARS1*-3xFLAG. The reciprocal immunoprecipitation was also performed by immunoprecipitating *AARS1*-3xFLAG and immunoblotting for *AARS1*-6xHis. Both approaches detected comparable interactions between wild-type and wild-type, wild-type and G102R and wild-type and R329H *AARS1* (Fig. 2B and C). These co-immunoprecipitations demonstrate that neither R329H nor

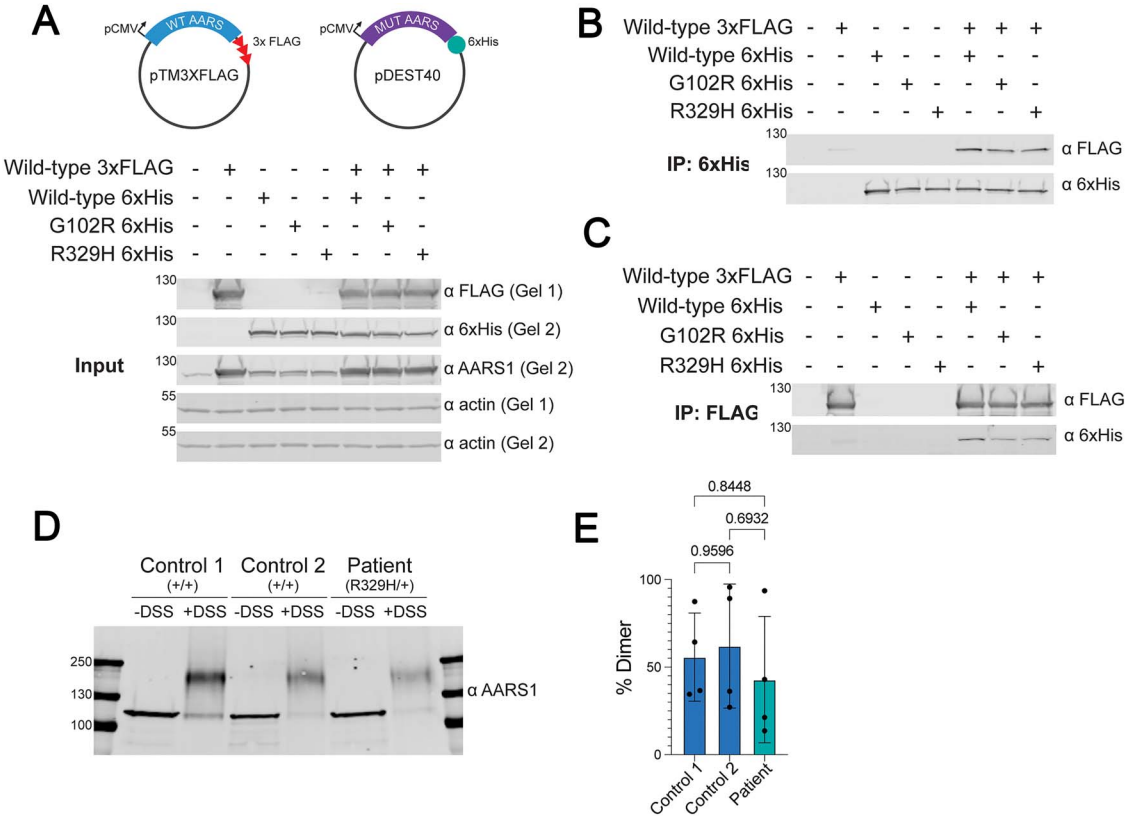

Figure 2. G102R and R329H *AARS1* dimerize with wild-type *AARS1*. (**A**) HEK293T cells were transfected with vectors to co-express wild-type and mutant human *AARS1*, and a western blot was performed to detect the resulting proteins along with endogenous loading controls. The image is representative of three independent replicates. A cartoon along the top illustrates the constructs employed in the experiments, and the presence or absence of each construct is indicated across the top of the gel image. Protein molecular weights are indicated in kilodaltons (kDa) along the left side of the image and antibodies are indicated along the right side. (**B**) After immunoprecipitation with an anti-6xHis antibody, a western blot was performed to detect co-immunoprecipitated proteins. A representative image from five (for R329H) or three (for G102R) independent replicates are shown. This image is annotated as in panel A. (**C**) After immunoprecipitation with an anti-FLAG antibody, a western blot was performed to detect co-immunoprecipitated proteins. A representative image from two independent replicates is shown. This image is annotated as in panels A and B. (**D**) After treating patient and control samples with a protein cross-linking agent, a western blot was performed to detect endogenous *AARS1* protein. The image is representative of four independent technical replicates. Samples and conditions are indicated across the top of the image, protein molecular weights are indicated in kilodaltons (kDa) along the left side, and the antibody employed is indicated on the right side. DSS = disuccinimidyl suberate. (**E**) The percentage of dimeric *AARS1* protein signal in the total *AARS1* protein signal (D) was quantified with ImageJ. The mean of four technical replicates is shown, with error bars representing one standard deviation. A one-way ANOVA with Tukey's multiple comparisons tests [$F(2,9) = 0.3602$, $P = 0.7071$] was performed to determine if there was a statistically significant difference between R329H/+ cells and either of the two controls.

G102R ablates dimerization with the wild-type *AARS1* subunit. As a complementary approach, the total dimerization of endogenous *AARS1* was studied using an R329H/+ patient cell line. Patient fibroblasts were crosslinked with disuccinimidyl suberate (DSS), along with two independent control fibroblast cell lines. In untreated technical replicates (-DSS), *AARS1* protein is detected between 100 and 130 kDa, consistent with its predicted size of 107 kDa. In DSS-treated technical replicates, an additional band migrates at approximately twice the molecular weight, consistent with a dimeric *AARS1* protein (Fig. 2D). The percentage of *AARS1* in dimeric form was not significantly different between the control line and the patient cell line (Fig. 2E). Combined, the above data indicate that mutant *AARS1* proteins retain the ability to dimerize with wild-type *AARS1*, which is required for a dominant-negative effect.

Engineering dimer-disrupting *AARS1* variants

If neuropathy-associated *AARS1* variants (e.g. R329H or G102R) act in a dominant-negative manner, then introducing a dimer-disrupting variant in *cis* with the pathogenic variant should reduce interactions between mutant and wild-type *AARS1* proteins, temper any dominant-negative effects and rescue the observed reduction in yeast cell growth. To identify dimer-disrupting variants, a series of deletions were designed in the C-terminal domain of *AARS1* based on the published crystal structure (52). The C-terminal domain is predicted to be essential for *AARS1* dimerization, although it has been shown to be dispensable for *AARS1* expression and tRNA charging activity *in vitro* (53). Engineered deletions in this domain targeted amino acids that have multiple contacts with the opposite subunit (Fig. 3A, left). This series comprised a seven amino acid deletion to encompass several contact points (K943_Q949del) as well as smaller deletions within or near this region (N944_G946del and Q949_E950del). This series also included the deletion of a single codon, which encodes C947, a cysteine residue that forms a putative disulfide bond with C773 on the opposite subunit (53). Finally, a stop codon at Q855 was introduced to ablate the 113 amino-acid residues of the terminal globular domain (Fig. 3A, right).

To assess the ability of each of the five putative dimer-disrupting *AARS1* alleles to support yeast growth in isolation, each allele was cloned into the pAG425 vector and transformed into the

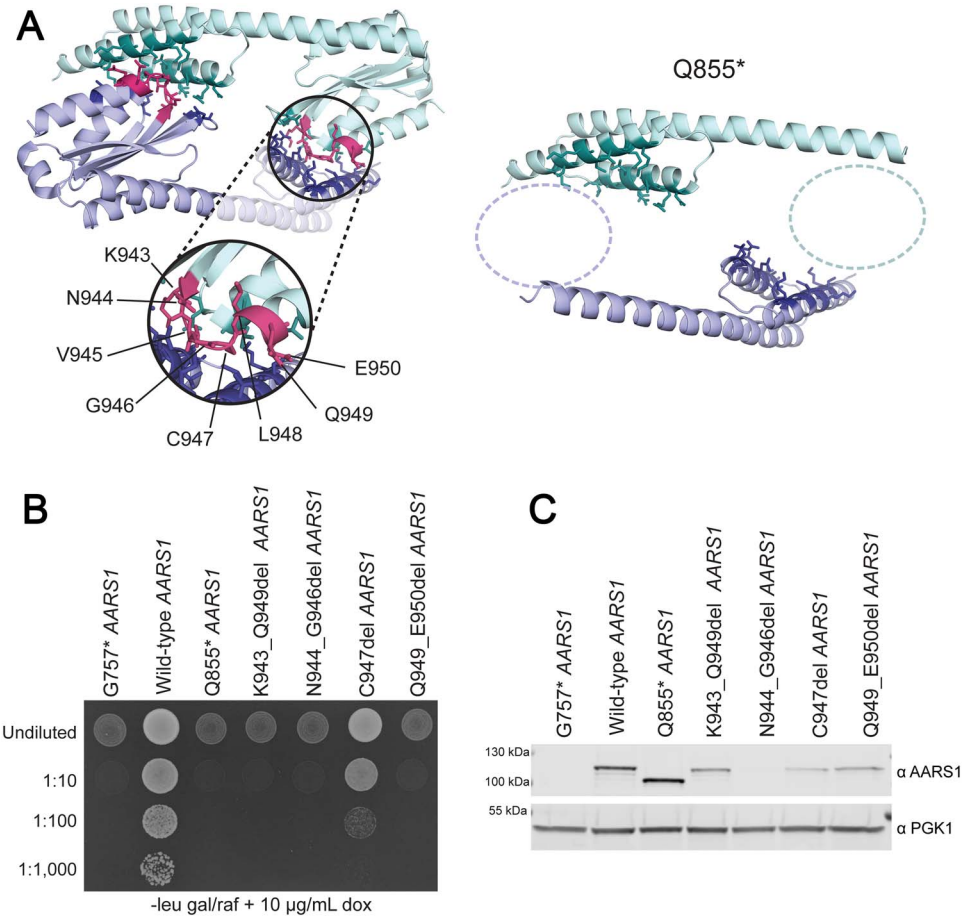

Figure 3. Engineering dimer-reducing *AARS1* variants. (**A**) A cartoon generated from PyMOL illustrates the crystal structure of the *AARS1* C-terminal dimerization domain (left side). One subunit from the dimer is shown in green, and the other in purple. Amino-acid residues that contact the opposite subunit are shown in dark green or dark purple. The residues targeted in this assay are shown in pink and labeled in the inset. On the right side of this panel is a second cartoon that illustrates the *AARS1* C-terminal dimerization domain with the Q855* mutation. The dashed circles indicate the globular domain that is ablated by the premature stop codon. (**B**) Yeast harboring a doxycycline-repressible endogenous *ALA1* locus were transformed with a pAG425 vector to express either wild-type or mutant human *AARS1* (i.e. one of the engineered mutations affecting the residues highlighted in panel A). Cultures were plated undiluted or diluted on media lacking leucine, and containing galactose/raffinose and doxycycline. A representative image of four biological replicates is shown. The dilution of the spotted yeast cultured is indicated on the left and the media conditions are indicated across the bottom (leu = leucine; gal = galactose; raf = raffinose; dox = doxycycline). (**C**) Yeast protein lysates were subjected to western blot analysis to detect the human *AARS1* proteins expressed from wild-type and mutant expression constructs, which are indicated across the top. Yeast was grown in galactose and raffinose media lacking leucine, with no doxycycline. A representative image of three biological replicates is shown.

ptetO7-*ALA1* yeast strain, followed by a complementation growth assay as described above. Interestingly, none of the deletions fully complemented the loss of *ALA1* (Fig. 3B), indicating that the affected residues are indeed important for *AARS1* protein function. To determine if the engineered mutations impact protein stability, each allele was evaluated for an effect on *AARS1* protein levels via western blot analysis. The N944_G946del allele led to no detectable *AARS1* protein (Fig. 3C), providing an explanation for its failure to complement in yeast. The C947 deletion significantly reduced *AARS1* expression (Fig. 3C), but still showed partial complementation in yeast (Fig. 3B), suggesting that this residue may be important for protein stability. The deletions K943_Q949del and Q949_E950del similarly reduced *AARS1* levels (Fig. 3C) and led to less yeast growth than C947del (Fig. 3B), suggesting that these deletions reduce function as well as protein abundance. Only the globular domain deletion Q855* resulted in a complete loss of yeast cell growth (Fig. 3B) with no detectable decrease in protein levels (Fig. 3C). Additionally, this mutation is not predicted to significantly alter the structure of the protein outside of the dimerization domain (Supplementary Material, Fig. S5). Based on these data we concluded that Q855* is the most appropriate allele to test for reduced dimerization.

To test if Q855* reduces binding to wild-type *AARS1*, HEK293T cells were transfected with wild-type *AARS1*-3xFLAG and either wild-type or Q855* *AARS1*-6xHis. First, all transfections resulted in robust *AARS1* protein expression (Fig. 4A), consistent with Q855* *AARS1* not significantly impacting protein levels. Second, immunoprecipitation of wild-type *AARS1*-6xHis co-precipitated wild-type *AARS1*-3xFLAG, confirming an interaction between the two tagged wild-type subunits (Fig. 4B). However, immunoprecipitation for Q855* *AARS1*-6xHis did not co-precipitate wild-type *AARS1*-3xFLAG (Fig. 4B), indicating that Q855* reduces or ablates binding to the wild-type *AARS1* protein. These findings were supported by performing the reciprocal experiment. Here, immunoprecipitation of wild-type *AARS1*-3xFLAG co-immunoprecipitated wild-type *AARS1*-6xHis, but did not co-immunoprecipitate Q855* *AARS1*-6xHis (Fig. 4C). These data demonstrate that the engineered Q855* *AARS1* variant reduces the interaction with wild-type *AARS1*, and for the first time

experimentally confirms that the C-terminal globular domain is required for dimerization.

Reducing the dimerization capacity of pathogenic *AARS1* alleles rescues yeast growth

If G102R and R329H *AARS1* act as dominant-negative alleles, then reducing the dimerization between mutant and wild-type *AARS1* proteins should rescue the mutation-associated depletion of yeast growth reported above. To test this, the Q855* mutation was introduced in *cis* with either G102R or R329H using site-directed mutagenesis. These double mutants were then cloned into pAG425 and transformed into the ptetO7-*ALA1* strain. Both G102R + Q855* *AARS1* and R329H + Q855* *AARS1* produced a truncated *AARS1* protein at levels comparable to wild-type *AARS1* (Supplementary Material, Fig. S6A and B).

Complementation assays expressing G102R + Q855* *AARS1* or R329H + Q855* *AARS1* in the presence of an empty p413 vector showed no yeast growth, consistent with the double-mutants acting as loss-of-function alleles (Fig. 5A). These alleles were then tested in the presence of wild-type *AARS1* expressed from the p413 vector. As before, neither the control allele G757* *AARS1* nor wild-type *AARS1* repressed yeast growth, and both G102R and R329H repressed yeast growth (Fig. 5B and C). Importantly, placing Q855* in *cis* with either G102R or R329H ameliorated the growth phenotype and increased the mean growth 24-fold or 82-fold respectively, or to 49% or 85% of wild-type levels (Fig. 5B and C). This rescued growth was comparable to that of yeast expressing the G757* control allele or wild-type *AARS1* in this experiment (Fig. 5C). These data demonstrate that disrupting the dimerization of G102R or R329H with wild-type *AARS1* is sufficient to rescue the dominant growth phenotype and show that the reduced growth phenotype is a result of mutant *AARS1* dimerizing with wild-type *AARS1*. In sum, these data provide evidence that neuropathy-associated *AARS1* alleles are loss-of-function variants that bind to and interfere with the function of wild-type *AARS1*; i.e. that they act via a dominant-negative mechanism.

Sequences that encode the *AARS1* anticodon-binding domain are susceptible to recurrent dominant-negative mutations

If G102R and R329H *AARS1* are dominant-negative alleles, it is likely that other neuropathy-associated *AARS1* variants act via this mechanism. To investigate this possibility, we focused on the R329 residue and the surrounding *AARS1* coding region. Previous work by McLaughlin *et al.* identified a high degree of cytosine methylation in this area, making it susceptible to cytosine deamination. This study predicted numerous missense variants that could arise from such C➔T changes (45). One such predicted change, R326W, was later found in a multi-generational family with CMT (24). Here, we report four additional individuals with mutations at the R329 residue, all of whom were examined by a neurologist and presented with axonal neuropathy (Supplementary Material, Table 1). One individual is heterozygous for R329S, a previously unreported variant that was predicted by the cytosine methylation analysis (45). The other three individuals comprise the eleventh family with CMT caused by the R329H variant, further strengthening the argument that this is a pathogenic allele and that the R329 residue is subject to recurrent mutation. In addition to R329H and R329S, McLaughlin *et al.* predicted that R329C could arise at this residue; however, this allele has yet to be identified in patients with CMT disease. Therefore, we assessed all three variants (R326W, R329S and R329C) in our yeast dominant-negative assay.

The R326W, R329S and R329C variants were introduced into the *AARS1* open reading frame with site-directed mutagenesis, then cloned into the galactose-inducible pAG425 expression vector and transformed into the ptetO7-*ALA1* yeast strain. G757* and wild-type *AARS1* were included as controls. To determine if our yeast model can distinguish between pathogenic and non-pathogenic *AARS1* alleles, we also tested G931S *AARS1*, which is a benign polymorphism found in the general population (with a gnomAD allele count of 2147 out of 282 842 chromosomes including 20 homozygous individuals (53). As previously reported (24), R326W did not support yeast growth in the absence of *ALA1* (Fig. 6A). Consistent with the functional importance of this region, R329S and R329C also did not support yeast growth (Fig. 6A). In contrast, G931S *AARS1* supported robust yeast cell growth, consistent with this being a benign allele. R326W, R329S and R329C *AARS1* were then tested in the presence of the wild-type *AARS1* allele expressed from p413. All three alleles repressed yeast growth in the presence of wild-type *AARS1*, compared to G757*, wildtype and G931S *AARS1* (Fig. 6B). Notably, this growth defect was improved by restoring the expression of endogenous *ALA1* (Supplementary Material, Fig. S3C and D), supporting the argument that the phenotype is due to an alanine-tRNA charging defect.

To determine if the dominant growth repression associated with these three alleles depends on their ability to dimerize with wild-type *AARS1*, the dimer-disrupting Q855* variant was introduced *in cis* with either R326W, R329S or R329C. These double-mutant alleles were transformed into yeast expressing an empty p413 vector, or expressing wild-type *AARS1* from p413. Strains were then plated on galactose (to express the double-mutant *AARS1* allele) and doxycycline (to repress endogenous *ALA1*). In the presence of the empty p413 vector, the double-mutants showed no yeast growth, consistent with the double-mutants acting as loss-of-function alleles (Fig. 7A). However, when co-expressed with wild-type *AARS1*, Q855* in *cis* with R329C, R329S or R326W rescued the repressed yeast growth for all three variants, increasing growth 15-fold, 26-fold and 29-fold, respectively (or to 90%, 93% and 73% of wild-type levels) (Fig. 7B and C). The growth of the double-mutants was not significantly different from the growth of the yeast expressing the control allele G757* or wild-type *AARS1* (Fig. 7C). Combined, these data indicate that R326W, R329S and R329C have dominant-negative properties. Together with G102R and R329H, this study presents evidence that neuropathy-associated *AARS1* variants act via a dominant-negative mechanism.

Discussion

In this study, we developed a yeast assay to study the molecular mechanism of neuropathy-associated *AARS1* alleles. We demonstrate that multiple pathogenic, loss-of-function *AARS1* variants repress yeast growth when co-expressed with the wild-type *AARS1* allele. We also show that these variants retain the ability to dimerize with the wild-type *AARS1* protein and that disrupting this interaction is sufficient to rescue the repressed yeast growth. These data provide evidence that neuropathy-associated *AARS1* alleles act via a dominant-negative mechanism that represses the activity of wild-type *AARS1*.

It will be important to employ the dominant-negative yeast model reported here to study other variants in *AARS1*. These studies will enable rapid characterization of newly identified *AARS1* alleles and will provide functional evidence supporting pathogenicity. Furthermore, an unbiased, massively parallel

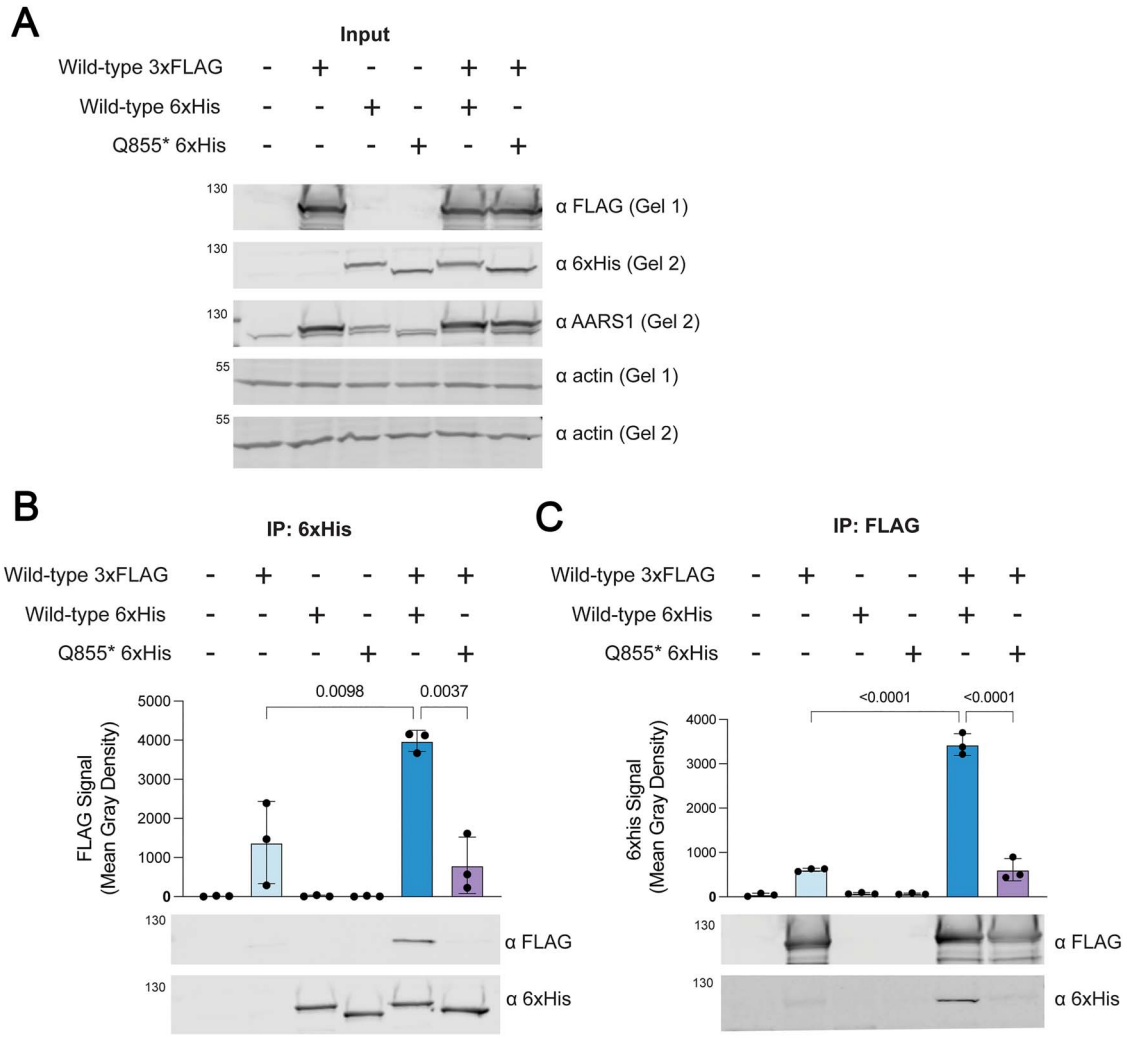

Figure 4. Q855* *AARS1* impairs dimerization with wild-type *AARS1*. (**A**) HEK293T cells were transfected with vectors to co-express wild-type or Q855* human *AARS1*, and a western blot was performed to detect the resulting proteins, as well as endogenous loading controls. The image is representative of three independent replicates. The presence or absence of each construct is shown across the top of the image, protein molecular weights are indicated in kilodaltons (kDa) along the left side, and antibodies are indicated along the right side. (**B**) After immunoprecipitation with an anti-6xHis antibody, a western blot was performed to detect co-immunoprecipitated proteins. The presence or absence of each construct is indicated at the top of the panel, and a representative image from three independent replicates is shown at the bottom of the panel (with annotation as in panel A). The middle of the panel shows ImageJ quantification of a 3xFLAG-tagged *AARS1* signal. Bars indicate the mean value and one standard deviation for three biological replicates. A one-way ANOVA with Dunnett's multiple comparisons test was performed to determine statistical significance [$F(2,6) = 15.21$, $P = 0.0045$]. (**C**) After immunoprecipitation with an anti-FLAG antibody, a western blot was performed to detect co-immunoprecipitated proteins. The panel is organized similarly to panel B, with ImageJ quantification of 6xHis-tagged *AARS1* signal in the middle of the panel. Bars indicate the mean value and one standard deviation for three biological replicates. A one-way ANOVA with Dunnett's multiple comparisons test was performed to determine statistical significance [$F(2,6) = 191.7$, $P < 0.0001$].

mutagenesis approach utilizing this model will help predict dominant-negative *AARS1* alleles that may be identified in patients in the future, such as R329C. This yeast model can also be adapted to study and predict pathogenic variants in *GARS1*, *HARS1*, *SARS1*, *YARS1* and *WARS1*. We hypothesize that pathogenic variants in these other neuropathy-associated ARS genes will also show dominant-negative effects because these genes also encode homo-dimeric ARS enzymes (53–56). Classifying pathogenic variants in these additional ARS loci as dominant-negative alleles will also contribute to defining a common mechanism of ARS-mediated dominant neuropathy, and will provide critical insight into how missense ARS variants lead to depleted pools of charged tRNA, which ultimately impairs protein translation (37,39–41).

Although the data presented here argue in favor of a dominant-negative effect, it is possible that dominant-negative and neomorphic gain-of-function effects work in concert to exacerbate neuronal pathology. A recent study showed that the pathogenic *AARS1* variants N71Y, G102R and R329H each cause a conformational change that enables binding to Neuropilin-1 (33), a widely expressed receptor that modulates a variety of signaling pathways and that is critical for neurovascular development (57). Such an interaction might compound the damage in patient neurons; however, the phenotype in our *AARS1* yeast model—combined with emerging pan-cellular phenomena of ribosome stalling and activation of the integrated stress response in the context of neuropathy-associated ARS variants (37,39,41,42)—demonstrates that a neuron-specific interaction is not required to assess pathogenic *AARS1* alleles for disease-relevant, deleterious effects. The tissue-specific phenotype in CMT disease may be due to the reported sensitivity of peripheral neurons to activation of the integrated stress response (41), which could be elicited

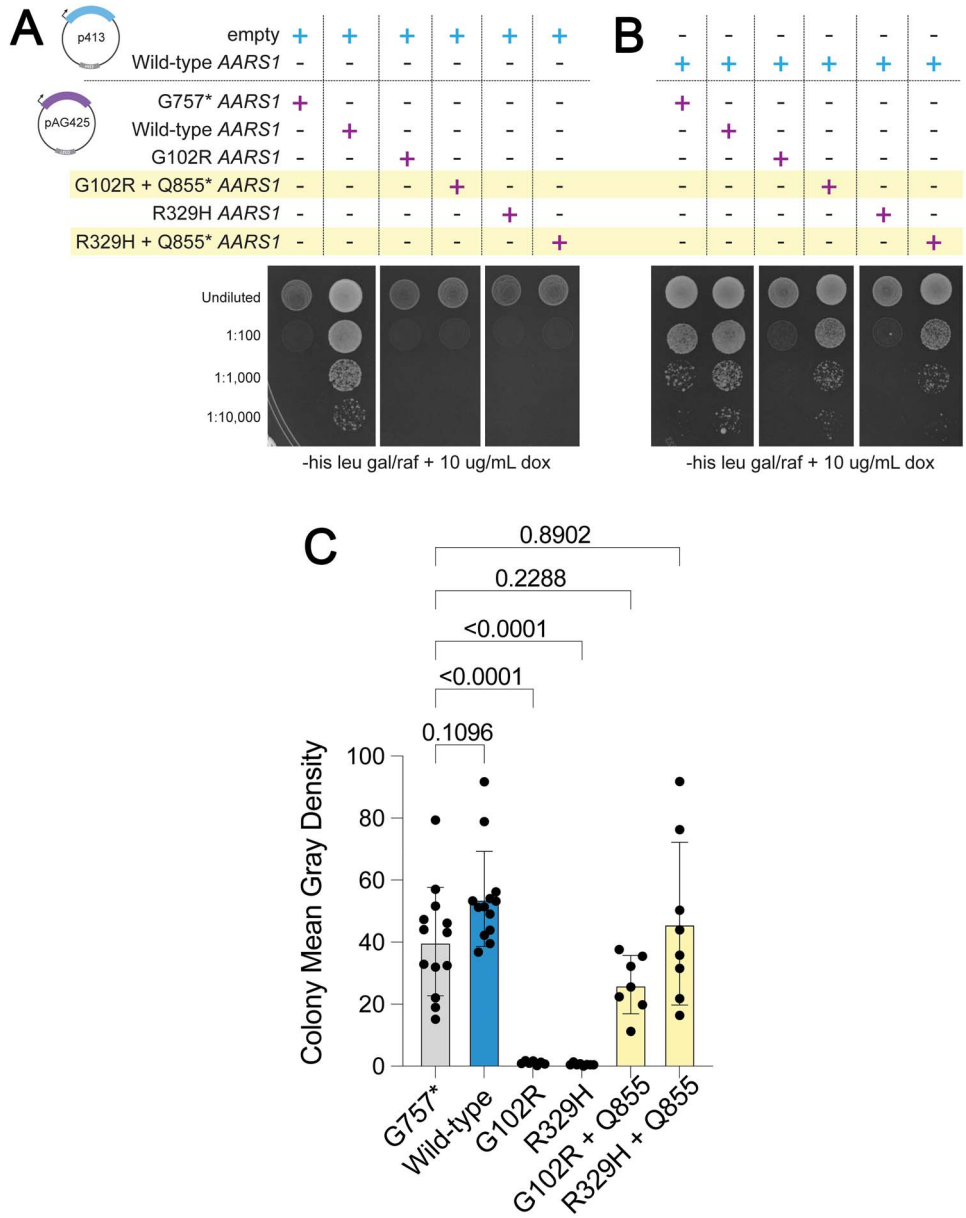

Figure 5. Reducing dimerization of G102R and R329H with wild-type *AARS1* rescues yeast growth. (**A**) Yeast with the doxycycline-repressible endogenous *ALA1* locus was transformed with an empty p413 vector and a pAG425 vector expressing wild-type or mutant human *AARS1*. Cultures were plated undiluted or diluted on media lacking histidine and leucine, and containing galactose/raffinose and doxycycline. (**B**) Similar to strains shown in panel A, except that yeast was transformed with p413 expressing wild-type human *AARS1*. For both panels, the vectors present in each experiment are indicated across the top, the dilution of the spotted yeast cultured is indicated on the left, and the media conditions are indicated across the bottom (his = histidine; leu = leucine; gal = galactose; raf = raffinose; dox = doxycycline). (**C**) Yeast spot intensity was quantified using ImageJ. Bars represent the mean and one standard deviation. Thirteen biological replicates were assessed for G757* and wild-type *AARS1*, eight for R329H and R329H + Q855*, and seven for G102R and G102R + Q855*. The indicated fold-change between the G102R strain and the G102R + Q855* strain, and the fold-change between the R329H strain and the R329H + Q855* strain, were both calculated using the mean of each sample. To compare yeast growth to the strain expressing both wild-type and G757* *AARS1*, a one-way ANOVA with Dunnett's multiple comparisons test was performed [$F(5,50) = 19.90$, $P < 0.0001$].

by a dominant-negative effect causing decreased availability of charged tRNA and ribosomal stalling.

A limitation of our yeast model is that the allelic expression is intentionally skewed, with the pathogenic allele over-expressed relative to the wild-type allele. This does not accurately reflect the presumably equal expression of wild-type and mutant alleles in the tissues of a heterozygous patient. Therefore, any dominant-negative effects in patients are likely to be weaker than those demonstrated here, and less likely to have such dramatic consequences for cell viability. Indeed, such a tempered effect in patient cells is more consistent with the late-onset and tissue-restricted patient phenotype. A terminally differentiated peripheral neuron that must maintain local protein translation far from the soma may be particularly susceptible to even mild dominant-negative effects of an ARS mutation. To determine if a dominant-negative effect drives dominant *AARS1*-mediated peripheral neuropathy, a knock-in animal model (e.g. mouse or worm) with an axonal pathology is required. Then, a dimer-disrupting variant such as Q855* can be introduced *in cis* with the pathogenic allele to determine if this ameliorates the neuronal phenotype.

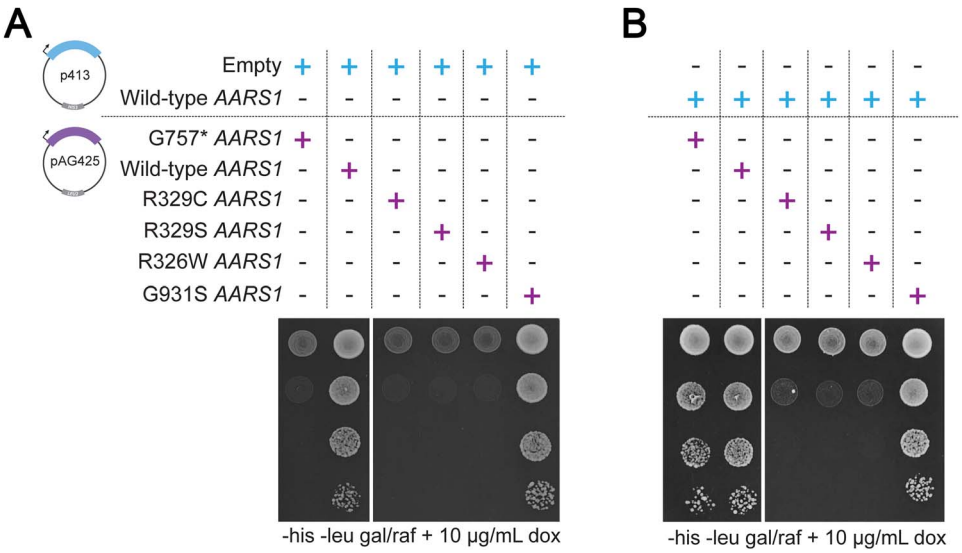

Figure 6. R329C, R329S and R326W *AARS1* are loss-of-function alleles that dominantly repress yeast cell growth. (**A**) Yeast with the doxycycline-repressible endogenous *ALA1* locus was transformed with a p413 vector with no insert, and a pAG425 vector expressing wild-type or mutant *AARS1*. Yeast cultures were spotted undiluted or diluted on media lacking histidine and leucine, and containing galactose/raffinose and doxycycline. (**B**) A similar experiment to that described in panel A, except that yeast expresses wild-type human *AARS1* from p413. For both panels, the vectors present in each experiment are indicated across the top, the dilution of the spotted yeast cultured is indicated on the left, and the media conditions are shown across the bottom (his = histidine; leu = leucine; gal = galactose; raf = raffinose; dox = doxycycline). Images are representative of three replicates.

It will also be important to determine if over-expressing wild-type *AARS1* will improve the neuronal phenotype, just as increasing *ALA1* expression mitigated the toxicity of the pathogenic *AARS1* alleles in yeast. If so, this may point to an important difference between the mechanism of *AARS1* mutations and the mechanism of certain *Gars1* mutations, where over-expressing wild-type *Gars1* did not rescue peripheral neuropathy in mice (36). This would be consistent with the different phenotypes associated with *AARS1* mutations and a subset of *GARS1* mutations, which can cause a more severe, earlier-onset, SMA-like phenotype (36). More generally, our study points to a difference between *AARS1* alleles and *GARS1* alleles, which have been shown to increase binding to tRNA, depriving the translation machinery of free-charged tRNA (39,42). Two previously reported observations to make it unlikely that the dominant toxicity of the *AARS1* alleles in yeast is related to tRNA sequestration: (1) the Q855* mutation that rescues toxicity in yeast is unlikely to impact tRNA binding because the C-terminal domain of human AARS1 does not efficiently bind tRNA (58); and (2) the R329 residue has been shown—through mutagenesis studies—to be essential for tRNA binding, making it unlikely that this mutation results in increased tRNA binding (59). However, the tRNA sequestration model has yet to be empirically tested for *AARS1* alleles. Furthermore, it will be important to determine if dimerization is relevant to other pathological models—including tRNA sequestration and Neuropilin-1 binding—by testing the Q855* allele *in cis* with the selected pathogenic alleles. To further delineate the differences and similarities between *GARS1* mechanisms and *AARS1* mechanisms, it would also be fruitful to test the known dimer-disrupting *GARS1* mutation T130K (60) *in cis* with dominant *Gars1* mutations to test if dimerization is required for the pathology. This experiment might also provide insight into any interplay between dominant-negative mechanisms and tRNA sequestration. It is possible that one mechanism exacerbates the other, or that both are independent but lead to similar downstream effects on protein translation.

Although there has been debate (33,52) as to whether *AARS1* functions as a dimer or a monomer, the results of our study demonstrate that it likely functions as a dimer *in vivo*, which is a requirement for a dominant-negative mechanism of disease. Two previous studies using purified *AARS1* protein for *in vitro* analyses concluded that it primarily exists as a monomer. One study (52) concluded that the C-terminal dimerization domain (beginning at G757) is dispensable for *in vitro* aminoacylation, while another (33) used gel filtration chromatography to show that the primary *in vitro* form is monomeric. However, our data demonstrate that, at least in an *in vivo* cellular context, the C-terminal dimerization domain is likely required for protein stability. Furthermore, we have shown that the globular domain beginning at Q855*, whereas not required to maintain protein levels in yeast or mammalian cells, is required for both *AARS1* dimerization and activity in yeast. This indicates that dimerization is necessary for *AARS1* function *in vivo*. Finally, chemically crosslinked *AARS1* from human fibroblast cells is detected at two molecular weights, one corresponding to a monomeric form and one corresponding to a dimeric form. Overall, these data reveal that *AARS1* dimerization is important for protein function *in vivo*.

To the best of our knowledge, there have been few yeast systems developed to test human pathogenic variants for a dominant-negative effect. Notable examples include reporter assays to test for dominant-negative p53 mutations (61,62) and enzymatic evaluation of yeast expressing dominant-negative UDP-galactose4-epimerase alleles (63,64). In general, yeast approaches are limited by the ability to recapitulate mammalian gene function in yeast cells. As such, they are best suited to study variants in genes with highly conserved functions, particularly ones that impact a readily observable phenotype, such as cellular growth. Using strategies like those presented here, variants in genes that fit these requirements can be efficiently interrogated for loss-of-function and/or dominant-negative properties, providing critical data to aid in patient

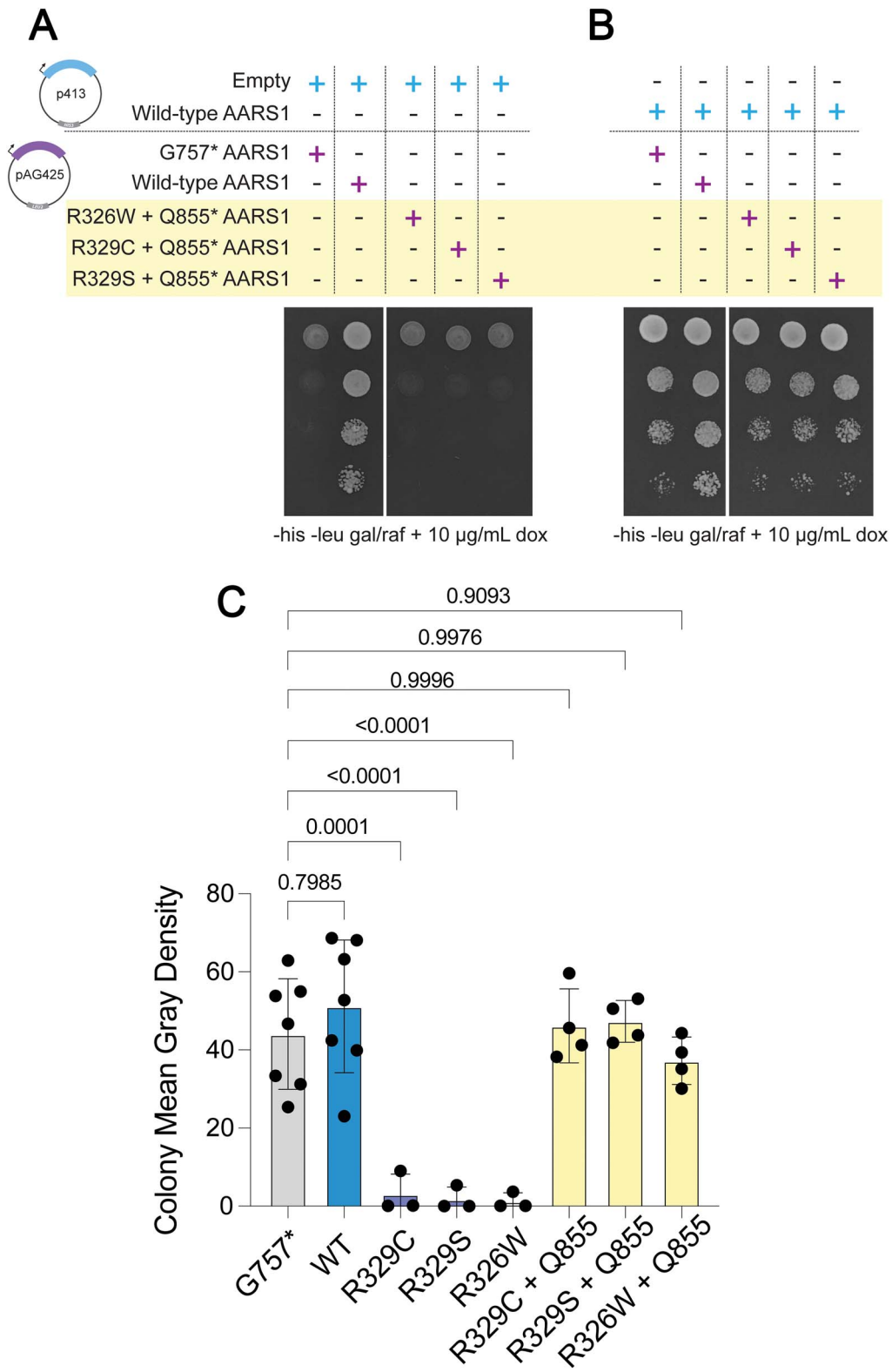

Figure 7. Reducing dimerization of R329C, R329S or R326W with wild-type *AARS1* rescues yeast growth. (**A**) Yeast with the doxycycline-repressible *ALA1* locus was transformed with an empty p413 vector and a pAG425 vector expressing either wild-type or mutant *AARS1*. Yeast was spotted undiluted or diluted on media lacking histidine and leucine, and containing galactose/raffinose and doxycycline. (**B**) An experiment similar to that described in panel A, except that yeast expresses wild-type human *AARS1* from the p413 vector. (**C**) Yeast spot intensity was quantified using ImageJ analysis; bars represent the mean and one standard deviation. At least three biological replicates were assessed for all variants. The indicated fold change between the strains expressing R329C, R329S or R326W, and their counterpart with Q855* *in cis*, was calculated using the mean intensity of each condition. To compare yeast growth to that of the strain expressing both wild-type and G757* *AARS1*, a one-way ANOVA with Dunnett's multiple comparisons test was performed [$F(7,27) = 14.72$, $P < 0.0001$].

diagnosis and further defining how genetic variation impacts gene function.

Here, we describe a tractable yeast model for rapidly evaluating variants in aminoacyl-tRNA synthetase genes for a dominant-negative effect. We demonstrate that multiple well-characterized, pathogenic *AARS1* variants repress yeast growth when co-expressed with wild-type *AARS1*, but that this phenotype is rescued when the mutant subunit is prevented from dimerizing with the wild-type subunit. This work presents the first direct evidence that pathogenic ARS alleles have dominant-negative properties, which may contribute to the effect of neuropathy-associated ARS variants by reducing the availability of charged tRNA, causing ribosome stalling, and triggering the integrated stress response (as shown for neuropathy-associated *HARS1* [37] and *GARS1* alleles [39,41,42]). In sum, this work contributes to further delineating the molecular mechanism of ARS-mediated dominant peripheral neuropathy.

Materials and Methods

Yeast vector construction and growth assays

All yeast assays were performed using the haploid ptetO7-*ALA1* strain from the Yeast Tet-Promoters Hughes Collection (YSC1180-202219317, Horizon Discovery). *AARS1* variants were generated using site-directed mutagenesis (Agilent QuikChange II XL Site-Directed Mutagenesis Kit) against the *AARS1* open reading frame in pDONR221 (primers available upon request). All clones were verified via Sanger sequencing. The Gateway cloning (Invitrogen) LR reaction was used to recombine the wild-type or mutant *AARS1* locus into pAG425GAL-ccdB (Addgene #14153). This is a Gateway-compatible vector with a 2-μm origin of replication that produces a high vector copy number per cell, a *GAL1* promoter that drives high expression of the target gene in a galactose-inducible fashion, and a *LEU2* auxotrophic marker.

To assess the function of *AARS1* variants independent of wild-type *AARS1*, a p413 vector (ATCC #87370) with no *AARS1* insert ('Empty') was introduced into the ptetO7-*ALA1* strain using lithium acetate yeast transformation. The p413 vector contains an *ADH1* promoter to drive constitutive expression of the target gene, a centromeric origin of replication to produce a low plasmid copy number per cell, and a *HIS3* auxotrophic marker for selection. This transformation was followed by a second transformation to introduce a pAG425 vector harboring wild-type or mutant *AARS1* (see above). Colonies were grown on media lacking histidine and leucine (DO Supplement -His/-Leu, Takara Bio) to select for the presence of both vectors. After transformation, colonies were grown in 2 ml liquid media in a 14 ml round-bottom conical tube (Fisher Scientific) for 2 days at 30°C, shaking at 275 rpm (on an I-24 incubator shaker, New Brunswick Scientific) until saturated. Yeast was then diluted 1:10, 1:100 and 1:1000 in water. 10 μl of undiluted or diluted samples were spotted on plates containing glucose, galactose/raffinose (Takara Bio Minimal SD Bases) or galactose/raffinose with 10 μg/ml doxycycline (Fisher Scientific BP26531). Plates were imaged after four days of growth.

To co-express mutant and wild-type *AARS1* in yeast, Gateway Cassette C (Invitrogen) was cloned into the p413 vector just downstream of (3′ to) the *ADH1* promoter using the *SmaI* restriction site. Clones were sequence verified to confirm the correct orientation. The LR Gateway reaction was then used to recombine wild-type *AARS1* from pDONR221 into p413. This construct was transformed into the ptetO7-ALA1 strain, followed by *AARS1* (wild-type or mutant) in pAG425. Yeast was grown and spotted as detailed above. All growth assays (studying a single *AARS1* allele or two co-expressed *AARS1* alleles) were performed side-by-side with the same pAG425 plasmid aliquots to enable direct comparisons. To quantitatively analyze yeast spots, the mean gray values of each spot were obtained using ImageJ, according to a previously published protocol (65).

Yeast protein isolation

To assess the expression of each human *AARS1* protein in yeast, the ptetO7-*ALA1* strain was transformed with a vector (pAG425) to express wild-type or mutant *AARS1* and grown on media lacking leucine (DO Supplement -Leu, Takara Bio). One colony was picked, placed into 3 ml media, and grown for 2–3 days shaking at 275 rpm at 30°C until saturated, reaching an optical density (OD_{600}) of approximately 2. Yeast was then centrifuged at 1000×g for 10 min, washed once with water, transferred to a 1.5 ml Eppendorf tube, then centrifuged at 21 130×g for 1 min. The supernatant was removed and the pellet was stored at −80°C. The pellet was thawed in 150 μl yeast lysis buffer (50 mM Na-HEPES pH 7.5, 100 mM NaOAc, 1 mM EDTA, 1 mM EGTA, 5 mM MgOAc, 5% glycerol, 0.25% NP-40 and 3 mM DTT) with 1X Halt Protease Inhibitor Cocktail (Thermo Fisher Scientific). Approximately 100 μl of 0.5 mm cold glass beads (Biospec Products) were added to each sample. Samples were vortexed at 4°C for 3 min, followed by 2 min resting on ice, followed by 3 min of vortexing at 4°C. To remove the lysate from the beads, a 26-gauge needle (BD PrecisionGlide) was used to make a hole in the bottom of the 1.5 ml tube, which was then immediately inserted into a 14 ml round bottom conical tube. Lysates were centrifuged at 200×g at 4°C for 5 min. The lysates were collected from the bottom of the conical tube and transferred to a 1.5 ml Eppendorf tube and were then centrifuged at 16, 363×g for 5 min at 4°C. Supernatants were collected and protein concentrations were measured using the Thermo Scientific Pierce BCA Protein Assay kit, and 50 μg of protein per sample was used for western blot analysis (see below).

Co-immunoprecipitation of wild-type *AARS1* and mutant *AARS1*

To test for interactions between wild-type and mutant *AARS1* proteins we performed co-immunoprecipitation followed by western blot analysis in cultured mammalian cells. The LR Gateway reaction was used to recombine the wild-type or mutant *AARS1* open reading frame from pDONR221 into pDEST40 (Thermo Fisher Scientific) or pTM3xFLAG (gift from Moran Laboratory, University of Michigan). These vectors allow differential tagging of the mutant and wild-type *AARS1* alleles; wild-type *AARS1*-3xFLAG (a C-terminal tag) was expressed from pTM3xFLAG using a CMV promoter, and either wild-type or mutant *AARS1*-6xHis (a C-terminal tag) was expressed from pDEST40 using a CMV promoter. 100 mm plates (Falcon) were seeded with 1.5–2 million HEK293T cells; the following day, these were transfected with 0.5 pmol plasmid using Lipofectamine 3000 (Invitrogen). Forty-eight hours after transfection, cells were harvested using Trypsin–EDTA (Gibco, Fisher Scientific) and centrifuged at 800×g for 2 min at 4°C. Cells were then washed once with 1X PBS (Thermo Fisher Scientific), centrifuged again (as above), and then resuspended in 1 ml lysis buffer (20 mM Tris–HCl pH 8, 137 mM NaCl, 2 mM EDTA, 1% NP-40 and 0.25% sodium deoxycholate) with 1X Halt Protease Inhibitor Cocktail (Thermo Fisher Scientific). Samples were incubated for 2 h, rocking at 4°C, then centrifuged for 15 min at 16 363×g at 4°C. The supernatant was collected and protein concentration was measured using the Thermo Scientific Pierce BCA Protein Assay kit.

To conjugate beads with individual antibodies, 25 μl of Dynabeads Protein G (Fisher Scientific) were aliquoted per sample. All immunoprecipitations were performed using a MagnaRack (Invitrogen). Each aliquot was washed twice with 500 μl conjugation buffer (0.5% BSA, 0.1% Triton X-100 in PBS), then suspended in 500 μl conjugation buffer with 2 μg 6xHis antibody (Abcam 18 184) or 2 μg FLAG antibody (BioLegend 637 302). Beads and antibodies were incubated overnight with rocking at 4°C.

Before immunoprecipitation, lysates were pre-cleared to remove any proteins with non-specific affinity for the magnetic beads. An additional 25 μl of Dynabeads per sample was aliquoted and washed once with lysis buffer. Then, 1 mg of cell lysate in 500 μl lysis buffer was added to the beads and rocked at 4°C for 2 h. Supernatant from the antibody-conjugated beads was then removed, and the pre-cleared lysates were added. Samples were incubated for 3 h rocking at 4°C. For anti-6xHis IPs, samples were washed four times with 1 ml high salt buffer (10 mM Tris–HCl pH 7.5, 400 mM NaCl, 1 mM EDTA, 1 mM EGTA and 0.5% NP-40). For anti-FLAG IPs, samples were washed three times with 1 ml low salt buffer (10 mM Tris–HCl pH 7.5, 137 mM NaCl, 1 mM EDTA, 1 mM EGTA and 0.5% NP-40). On the last wash, samples were moved to fresh 1.5 ml tubes to prevent co-elution of proteins bound to the tube walls. Samples were re-suspended in 50 μl wash buffer with 50 μl 2× Tris-Glycine Buffer (Invitrogen). About, 4 μl BME was added before samples were boiled at 99°C for 5 min and the supernatant was collected for western blot (see below). Samples were divided in half and loaded in duplicate for immunoblotting with anti-*AARS1*, anti-6xHis, or anti-FLAG.

Disuccinimidyl suberate crosslinking

To determine the degree of *AARS1* dimerization in patient cells, *AARS1* protein was crosslinked with disuccinimidyl suberate (DSS) and analyzed by western blot. Patient and control fibroblasts were grown at 37°C in 5% CO_2 and standard growth media (DMEM supplemented with 10% FBS, 2 mM L-glutamine, 100 U/ml penicillin and 50 μg/ml streptomycin [Invitrogen]). Approximately 1 million cells were harvested from each sample with Trypsin–EDTA (Gibco, Fisher Scientific) and centrifuged at 800×g for 2 min at 4°C. They were then washed once with 1X PBS (Thermo Fisher Scientific), transferred to a 1.5 ml tube, and centrifuged again (as above). Cells were then re-suspended in 50 mM HEPES 0.5% NP-40. The sample was divided in two and 50 mM DSS (Thermo Fisher Scientific) was added to one aliquot to a final concentration of 5 mM. Both aliquots were incubated at room temperature for 30 min. The crosslinking reaction was then quenched with a final concentration of 30 mM TrisCl pH 7.5 at room temperature for 15 min. Samples were centrifuged at 16 363×g for 10 min at 4°C, and the supernatant was collected for western blot analysis (see below). 20 μg of protein was analyzed for each sample. An antibody against human *AARS1* (Bethyl Laboratories A303-473A) was used at a dilution of 1:500.

Co-immunoprecipitation of wild-type ALA1 and wild-type *AARS1*

To investigate an interaction between yeast ALA1 and human *AARS1*, co-immunoprecipitation experiments were performed. First, the endogenous yeast *ALA1* coding sequence was amplified from a previously published (45) pDONR221 clone with or without a C-terminal 6xHis tag encoded in the reverse primer (primer sequences available upon request). Then, Gateway cloning was used to recombine these constructs into p413 (see above). The ptetO7-*ALA1* strain was transformed with p413 to express either 6xHis-tagged or untagged *ALA1*, then subsequently transformed with pAG425 to express either R329H or G757* human *AARS1*. Colonies were grown for 2–3 days until saturated in -leu -his liquid glucose growth medium, then washed in water and re-suspended in 125-250 ml -leu -his galactose liquid culture (Takara Bio Minimal SD Bases, Takara Bio DO Supplement -His/−Leu). Cultures were grown to saturation, then centrifuged at 1000×g at 4°C for 20 min. Yeast was washed with water and aliquoted evenly into 4–5 1.5-ml tubes. Each sample was then centrifuged at 21 130×g for 1 min. The supernatant was removed and pellets were stored at −80°C. The pellets were thawed in yeast lysis buffer (50 mM Na-HEPES pH 7.5, 100 mM NaOAc, 1 mM EDTA, 1 mM EGTA, 5 mM MgOAc, 5% glycerol, 0.25% NP-40 and 3 mM DTT) with 1X Halt Protease Inhibitor Cocktail (Thermo Fisher Scientific). Approximately 100 μl of buffer was used for each 100 mg of pellet. Cells were lysed using the methods detailed above.

About, 25 μl of Dynabeads Protein G (Fisher Scientific) were prepared for each of the samples. Beads were washed twice with 500 μl conjugation buffer (0.5% BSA, 0.1% Triton X-100 in PBS), then re-suspended in 500 μl buffer and 2 μg anti-*AARS1* (ab226259). Beads and antibodies were incubated overnight with rocking at 4°C. Yeast cell lysates were pre-cleared before immunoprecipitation: 25 μl of magnetic beads were aliquoted and washed once with lysis buffer before a 2 mg aliquot of yeast lysate in a total of 500 μl lysis buffer was added. Samples were incubated with rocking at 4°C for 1 h. The supernatant was then removed from antibody-conjugated beads and replaced with the pre-cleared lysates. These samples were then incubated with rocking for 2.5 h at 4°C. After incubation, samples were washed once with 500 μl lysis buffer, once with 200 μl lysis buffer, and then re-suspended in 100 μl lysis buffer before being transferred to a fresh 1.5 ml Eppendorf tube. The supernatant was then removed and beads were suspended in 25 μl lysis buffer and 25 μl 2× Tris-Glycine Buffer (Invitrogen). Samples were boiled for 5 min with 2 μl BME and supernatants were removed to analyze in western blot assays.

Western blot analyses

To assess the levels of specific proteins in each experiment, western blots were performed. Protein concentrations for each sample were measured using the Thermo Scientific Pierce BCA Protein Assay kit. Samples were prepared with 1X Novex Tris-Glycine SDS sample buffer (Invitrogen) and 2-mercaptoethanol (BME) and boiled at 99°C for 5 min. Protein samples were separated on precast 4–20% Novex Wedgewell Tris-glycine gels (Invitrogen) at 150 V for 1 h and 15 min. PVDF membranes (Millipore Sigma) were pre-washed in 100% methanol for 1 min, then soaked in 1X transfer buffer (Invitrogen) and 10% methanol between two pieces of filter paper (Thermo Fisher Scientific). The separated protein samples were transferred to the PVDF membranes using a Mini Trans-Blot Electrophoretic Transfer Cell (Biorad) at 100 V for 1 h. Membranes were then blocked for 1 h with a 5% milk powder solution in 1X TBST. Primary antibodies were applied in 5% milk and membranes were incubated by rocking overnight at 4°C. The following day, membranes were washed three times with 1X TBST. Secondary antibodies (Licor) against mouse (for the 6xHis primary antibody and the PGK1 primary antibody), rabbit (for the *AARS1* primary antibody and the actin primary antibody), or rat (for the FLAG primary antibody) were diluted in 5% milk powder solution at a concentration of 1:20 000, along with 0.1% Tween-20 and 0.02% SDS. This solution was applied to membranes for 1 h, rocking at room temperature. Membranes were then washed three

times with 1X TBST before exposure using a Licor Odyssey CLx Imaging System.

For yeast protein and HEK293T co-immunoprecipitation experiments, the *AARS1* antibody (Bethyl Laboratories A303-473A) was used at 1:1000 dilution. For fibroblast DSS assays, the same *AARS1* antibody was used at 1:500 dilution. For HEK293T and yeast co-immunoprecipitation experiments, the 6xHis antibody (Abcam 18 184) was used at a dilution of 1:3000. The FLAG antibody (BioLegend 637 302) was used at a 1:2500 dilution. The loading control was actin (Sigma A5060, 1:5000) for mammalian protein blots and PGK1 (Abcam ab113687, 1:3000) for yeast protein blots. For co-immunoprecipitation studies of *AARS1* and ALA1, the *AARS1* antibody used was Abcam ab226259 at a dilution of 1:500. Supplementary Material, Figures 7–9 show full-length western blots for data presented in Figures 2A–C, 3C, 4A–C.

AARS1 protein structure prediction

To predict whether Q855* significantly alters *AARS1* protein structure, the AlphaFold Colab notebook was used to predict the protein structure of the first 854 amino acids of *AARS1* (Uniprot P49588-1). To enable a sdirect comparison between mutant and wild-type, AlphaFold Colab was also used to predict the structure of the full-length *AARS1* amino acid sequence. Predicted structures were visualized and aligned using PyMOL.

Clinical and genetic evaluation of newly reported patients

All patients were evaluated as part of the Inherited Neuropathy Consortium natural history study (protocol 6601), which has received Institutional Review Board/Ethics Board approval for the study. All patients or their guardians signed consent forms. A Clinical Laboratory Improvement Amendments-certified laboratory in the United States performed all genetic testing.

Statistical data analysis

All statistical analyses were performed with GraphPad Prism. One-way ANOVAs with multiple comparison tests were used to determine statistical significance.

Supplementary Material

Supplementary Material is available at *HMG* online.

Acknowledgements

The authors would like to thank: Dr Thomas Glover and Dr Miriam Meisler for their gifts of fibroblast cell lines from unaffected individuals; Dr Thomas Wilson for advice on yeast genetic experimentation; Dr John Moldovan, Dr Trenton Frisbie and Dr Stephanie Moon for advice on protein–protein interaction experiments; and Dr John Moran for advice on protein biochemistry and yeast genetic studies, and frequent discussions on the goals of the study. The authors would also like to thank Alex Mark for his help running AlphaFold Colab, and Dr Laura Lavery for her advice on predicting protein structure.

Conflict of Interest statement. There is no conflict of interest to declare.

Funding

The National Institute of Health (NS108510 to R.M., GM136441 to A.A. and GM128836 to K.S.K.) and the Michigan Pre-doctoral Training in Genetics Program (GM007544 to R.M. and S.M.).

References

1. Shy, M.E., Lupski, J.R., Chance, P.F., Klein, C.J. and Dyck, P.J. (2005). Hereditary Motor and Sensory Neuropathies: An Overview of Clinical, Genetic, Electrophysiologic, and Pathologic Features. *In Peripheral Neuropathy: 2-Volume Set with Expert Consult Basic*, pp. 1623–1658. Elsevier. https://doi.org/10.1016/B978-0-7216-9491-7.50072-7.
2. Scherer, S.S., Kleopa, K.A. and Benson, M.D. (2020) Chapter 21 - Peripheral neuropathies. In Rosenberg, R.N. and Pascual, J.M. (eds), *Rosenberg's Molecular and Genetic Basis of Neurological and Psychiatric Disease, 6th edn*. Cambridge, MA: Academic Press, pp. 345–375.
3. Skre, H. (1974) Genetic and clinical aspects of Charcot-Marie-Tooth's disease. *Clin. Genet.*, **6**, 98–118.
4. Braathen, G.J., Sand, J.C., Lobato, A., Høyer, H. and Russell, M.B. (2011) Genetic epidemiology of Charcot-Marie-Tooth in the general population. *Eur. J. Neurol.*, **18**, 39–48.
5. Laura, M., Pipis, M., Rossor, A.M. and Reilly, M.M. (2019) Charcot-Marie-Tooth disease and related disorders: an evolving landscape. *Curr. Opin. Neurol.*, **32**, 641–650.
6. Antonellis, A. and Green, E.D. (2008) The role of aminoacyl-tRNA synthetases in genetic diseases. *Annu. Rev. Genomics Hum. Genet.*, **9**, 87–107.
7. Latour, P., Thauvin-Robinet, C., Baudelet-Méry, C., Soichot, P., Cusin, V., Faivre, L., Locatelli, M.-C., Mayençon, M., Sarcey, A., Broussolle, E. *et al.* (2010) A major determinant for binding and Aminoacylation of tRNAAla in cytoplasmic Alanyl-tRNA synthetase is mutated in dominant axonal Charcot-Marie-Tooth disease. *Am. J. Hum. Genet.*, **86**, 77–82.
8. Safka Brozkova, D., Deconinck, T., Griffin, L.B., Ferbert, A., Haberlova, J., Mazanec, R., Lassuthova, P., Roth, C., Pilunthanakul, T., Rautenstrauss, B. *et al.* (2015) Loss of function mutations in HARS cause a spectrum of inherited peripheral neuropathies. *Brain J. Neurol.*, **138**, 2161–2172.
9. Antonellis, A., Ellsworth, R.E., Sambuughin, N., Puls, I., Abel, A., Lee-Lin, S.-Q., Jordanova, A., Kremensky, I., Christodoulou, K., Middleton, L.T. *et al.* (2003) Glycyl tRNA synthetase mutations in Charcot-Marie-tooth disease type 2D and distal spinal muscular atrophy type V. *Am. J. Hum. Genet.*, **72**, 1293–1299.
10. He, J., Liu, X.-X., Ma, M.-M., Lin, J.-J., Fu, J., Chen, Y.-K., Xu, G.-R., Xu, L.-Q., Fu, Z.-F., Xu, D. *et al.* (2022) Heterozygous Seryl-tRNA synthetase 1 variants cause Charcot-Marie-Tooth disease. *Ann. Neurol.*, **93**, 244–256.
11. Tsai, P.-C., Soong, B.-W., Mademan, I., Huang, Y.-H., Liu, C.-R., Hsiao, C.-T., Wu, H.-T., Liu, T.-T., Liu, Y.-T., Tseng, Y.-T. *et al.* (2017) A recurrent WARS mutation is a novel cause of autosomal dominant distal hereditary motor neuropathy. *Brain*, **140**, 1252–1266.
12. Jordanova, A., Irobi, J., Thomas, F.P., Van Dijck, P., Meerschaert, K., Dewil, M., Dierick, I., Jacobs, A., De Vriendt, E., Guergueltcheva, V. *et al.* (2006) Disrupted function and axonal distribution of mutant tyrosyl-tRNA synthetase in dominant intermediate Charcot-Marie-tooth neuropathy. *Nat. Genet.*, **38**, 197–202.
13. Gonzalez, M., McLaughlin, H., Houlden, H., Guo, M., Yo-Tsen, L., Hadjivassilious, M., Speziani, F., Yang, X.-L., Antonellis, A., Reilly, M.M. *et al.* (2013) Exome sequencing identifies a significant

variant in methionyl-tRNA synthetase (*MARS*) in a family with late-onset CMT2. *J. Neurol. Neurosurg. Psychiatry*, **84**, 1247–1249.
14. Gillespie, M.K., McMillan, H.J., Kernohan, K.D., Pena, I.A., Meyer-Schuman, R., Antonellis, A. and Boycott, K.M. A novel mutation in MARS in a patient with Charcot-Marie-Tooth disease, axonal, type 2U with congenital onset. *J. Neuromuscul. Dis.*, **6**, 333–339.
15. Meyer-Schuman, R. and Antonellis, A. (2017) Emerging mechanisms of aminoacyl-tRNA synthetase mutations in recessive and dominant human disease. *Hum. Mol. Genet.*, **26**, R114–R127.
16. Kuo, M.E. and Antonellis, A. (2020) Ubiquitously expressed proteins and restricted phenotypes: exploring cell-specific sensitivities to impaired tRNA charging. *Trends Genet.*, **36**, 105–117.
17. Kuo, M.E., Theil, A.F., Kievit, A., Malicdan, M.C., Introne, W.J., Christian, T., Verheijen, F.W., Smith, D.E.C., Mendes, M.I., Hussaarts-Odijk, L. *et al.* (2019) Cysteinyl-tRNA synthetase mutations cause a multi-system, recessive disease that includes microcephaly, developmental delay, and brittle hair and nails. *Am. J. Hum. Genet.*, **104**, 520–529.
18. McLaughlin, H.M., Sakaguchi, R., Liu, C., Igarashi, T., Pehlivan, D., Chu, K., Iyer, R., Cruz, P., Cherukuri, P.F., Hansen, N.F. *et al.* (2010) Compound heterozygosity for loss-of-function lysyl-tRNA synthetase mutations in a patient with peripheral neuropathy. *Am. J. Hum. Genet.*, **87**, 560–566.
19. Manole, A., Efthymiou, S., O'Connor, E., Mendes, M.I., Jennings, M., Maroofian, R., Davagnanam, I., Mankad, K., Lopez, M.R., Salpietro, V. *et al.* (2020) De novo and Bi-allelic pathogenic variants in NARS1 cause neurodevelopmental delay due to toxic gain-of-function and partial loss-of-function effects. *Am. J. Hum. Genet.*, **107**, 311–324.
20. Seburn, K.L., Nangle, L.A., Cox, G.A., Schimmel, P. and Burgess, R.W. (2006) An active dominant mutation of glycyl-tRNA synthetase causes neuropathy in a Charcot-Marie-Tooth 2D mouse model. *Neuron*, **51**, 715–726.
21. Achilli, F., Bros-Facer, V., Williams, H.P., Banks, G.T., AlQatari, M., Chia, R., Tucci, V., Groves, M., Nickols, C.D., Seburn, K.L. *et al.* (2009) An ENU-induced mutation in mouse glycyl-tRNA synthetase (GARS) causes peripheral sensory and motor phenotypes creating a model of Charcot-Marie-Tooth type 2D peripheral neuropathy. *Dis. Model. Mech.*, **2**, 359–373.
22. Morelli, K.H., Griffin, L.B., Pyne, N.K., Wallace, L.M., Fowler, A.M., Oprescu, S.N., Takase, R., Wei, N., Meyer-Schuman, R., Mellacheruvu, D. *et al.* (2019) Allele-specific RNA interference prevents neuropathy in Charcot-Marie-Tooth disease type 2D mouse models. *J. Clin. Invest.*, **129**, 5568–5583.
23. Oprescu, S.N., Griffin, L.B., Beg, A.A. and Antonellis, A. (2017) Predicting the pathogenicity of aminoacyl-tRNA synthetase mutations. *Methods*, **113**, 139–151.
24. Weterman, M.A.J., Kuo, M., Kenter, S.B., Gordillo, S., Karjosukarso, D.W., Takase, R., Bronk, M., Oprescu, S., van Ruissen, F., Witteveen, R.J.W. *et al.* (2018) Hypermorphic and hypomorphic AARS alleles in patients with CMT2N expand clinical and molecular heterogeneities. *Hum. Mol. Genet.*, **27**, 4036–4050.
25. Bansagi, B., Antoniadi, T., Burton-Jones, S., Murphy, S.M., McHugh, J., Alexander, M., Wells, R., Davies, J., Hilton-Jones, D., Lochmüller, H. *et al.* (2015) Genotype/phenotype correlations in AARS-related neuropathy in a cohort of patients from the United Kingdom and Ireland. *J. Neurol.*, **262**, 1899–1908.
26. Lee, D.C., Meyer-Schuman, R., Bacon, C., Shy, M.E., Antonellis, A. and Scherer, S.S. (2019) A recurrent GARS mutation causes distal hereditary motor neuropathy. *J. Peripher. Nerv. Syst.*, **24**, 320–323.
27. Markovitz, R., Ghosh, R., Kuo, M.E., Hong, W., Lim, J., Bernes, S., Manberg, S., Crosby, K., Tanpaiboon, P., Bharucha-Goebel, D. *et al.* (2020) GARS-related disease in infantile spinal muscular atrophy: implications for diagnosis and treatment. *Am. J. Med. Genet.*, **182**, 1167–1176.
28. Abbott, J.A., Meyer-Schuman, R., Lupo, V., Feely, S., Mademan, I., Oprescu, S.N., Griffin, L.B., Alberti, M.A., Casasnovas, C., Aharoni, S. *et al.* (2018) Substrate interaction defects in histidyl-tRNA synthetase linked to dominant axonal peripheral neuropathy. *Hum. Mutat.*, **39**, 415–432.
29. Wang, B., Li, X., Huang, S., Zhao, H., Liu, J., Hu, Z., Lin, Z., Liu, L., Xie, Y., Jin, Q. *et al.* (2019) A novel WARS mutation (p.Asp314Gly) identified in a Chinese distal hereditary motor neuropathy family. *Clin. Genet.*, **96**, 176–182.
30. He, W., Bai, G., Zhou, H., Wei, N., White, N.M., Lauer, J., Liu, H., Shi, Y., Dumitru, C.D., Lettieri, K. *et al.* (2015) CMT2D neuropathy is linked to the neomorphic binding activity of glycyl-tRNA synthetase. *Nature*, **526**, 710–714.
31. Sleigh, J.N., Dawes, J.M., West, S.J., Wei, N., Spaulding, E.L., Gómez-Martín, A., Zhang, Q., Burgess, R.W., Cader, M.Z., Talbot, K. *et al.* (2017) Trk receptor signaling and sensory neuron fate are perturbed in human neuropathy caused by Gars mutations. *Proc. Natl. Acad. Sci. U.S.A.*, **114**, E3324–E3333.
32. Bervoets, S., Wei, N., Erfurth, M.-L., Yusein-Myashkova, S., Ermanoska, B., Mateiu, L., Asselbergh, B., Blocquel, D., Kakad, P., Penserga, T. *et al.* (2019) Transcriptional dysregulation by a nucleus-localized aminoacyl-tRNA synthetase associated with Charcot-Marie-Tooth neuropathy. *Nat. Commun.*, **10**, 5045.
33. Sun, L., Wei, N., Kuhle, B., Blocquel, D., Novick, S., Matuszek, Z., Zhou, H., He, W., Zhang, J., Weber, T. *et al.* (2021) CMT2N-causing aminoacylation domain mutants enable Nrp1 interaction with AlaRS. *Proc. Natl. Acad. Sci. U.S.A.*, **118**, 118.
34. Mo, Z., Zhao, X., Liu, H., Hu, Q., Chen, X.-Q., Pham, J., Wei, N., Liu, Z., Zhou, J., Burgess, R.W. *et al.* (2018) Aberrant GlyRS-HDAC6 interaction linked to axonal transport deficits in Charcot-Marie-Tooth neuropathy. *Nat. Commun.*, **9**, 1007.
35. Cui, Q., Bi, H., Lv, Z., Wu, Q., Hua, J., Gu, B., Huo, C., Tang, M., Chen, Y., Chen, C. *et al.* (2023) Diverse CMT2 neuropathies are linked to aberrant G3BP interactions in stress granules. *Cell*, **186**, 803–820.e25.
36. Motley, W.W., Seburn, K.L., Nawaz, M.H., Miers, K.E., Cheng, J., Antonellis, A., Green, E.D., Talbot, K., Yang, X.-L., Fischbeck, K.H. *et al.* (2011) Charcot-Marie-Tooth–linked mutant GARS is toxic to peripheral neurons independent of wild-type GARS levels. *PLoS Genet.*, **7**, e1002399.
37. Mullen, P., Abbott, J.A., Wellman, T., Aktar, M., Fjeld, C., Demeler, B., Ebert, A.M. and Francklyn, C.S. (2020) Neuropathy-associated histidyl-tRNA synthetase variants attenuate protein synthesis in vitro and disrupt axon outgrowth in developing zebrafish. *FEBS J.*, **288**, 142–159.
38. Nangle, L.A., Zhang, W., Xie, W., Yang, X.-L. and Schimmel, P. (2007) Charcot-Marie-tooth disease-associated mutant tRNA synthetases linked to altered dimer interface and neurite distribution defect. *Proc. Natl. Acad. Sci. U.S.A.*, **104**, 11239–11244.
39. Mendonsa, S., von Kuegelgen, N., Bujanic, L. and Chekulaeva, M. (2021) Charcot–Marie–Tooth mutation in glycyl-tRNA synthetase stalls ribosomes in a pre-accommodation state and activates integrated stress response. *Nucleic Acids Res.*, **49**, 10007–10017.
40. Niehues, S., Bussmann, J., Steffes, G., Erdmann, I., Köhrer, C., Sun, L., Wagner, M., Schäfer, K., Wang, G., Koerdt, S.N. *et al.* (2015) Impaired protein translation in drosophila models for Charcot–Marie–Tooth neuropathy caused by mutant tRNA synthetases. *Nat. Commun.*, **6**, 7520–7513.

41. Spaulding, E.L., Hines, T.J., Bais, P., Tadenev, A.L.D., Schneider, R., Jewett, D., Pattavina, B., Pratt, S.L., Morelli, K.H., Stum, M.G. *et al.* (2021) The integrated stress response contributes to tRNA synthetase–associated peripheral neuropathy. *Science*, **373**, 1156–1161.
42. Zuko, A., Mallik, M., Thompson, R., Spaulding, E.L., Wienand, A.R., Been, M., Tadenev, A.L.D., van Bakel, N., Sijlmans, C., Santos, L.A. *et al.* (2021) tRNA overexpression rescues peripheral neuropathy caused by mutations in tRNA synthetase. *Science*, **373**, 1161–1166.
43. Kachroo, A.H., Laurent, J.M., Yellman, C.M., Meyer, A.G., Wilke, C.O. and Marcotte, E.M. (2015) Evolution. Systematic humanization of yeast genes reveals conserved functions and genetic modularity. *Science*, **348**, 921–925.
44. Kachroo, A.H., Vandeloo, M., Greco, B.M. and Abdullah, M. (2022) Humanized yeast to model human biology, disease and evolution. *Dis. Model. Mech.*, **15**, dmm049309.
45. McLaughlin, H.M., Sakaguchi, R., Giblin, W., Wilson, T.E., Biesecker, L., Lupski, J.R., Talbot, K., Vance, J.M., Züchner, S., Lee, Y.-C. *et al.* (2012) A recurrent loss-of-function alanyl-tRNA synthetase (AARS) mutation in patients with Charcot-Marie-Tooth disease type 2N (CMT2N). *Hum. Mutat.*, **33**, 244–253.
46. Lee, A.J., Nam, D.E., Choi, Y.J., Nam, S.H., Choi, B.-O. and Chung, K.W. (2020) Alanyl-tRNA synthetase 1 (AARS1) gene mutation in a family with intermediate Charcot-Marie-Tooth neuropathy. *Genes Genom.*, **42**, 663–672.
47. Motley, W.W., Griffin, L.B., Mademan, I., Baets, J., De Vriendt, E., De Jonghe, P., Antonellis, A., Jordanova, A. and Scherer, S.S. (2015) A novel AARS mutation in a family with dominant myeloneuropathy. *Neurology*, **84**, 2040–2047.
48. Mnaimneh, S., Davierwala, A.P., Haynes, J., Moffat, J., Peng, W.-T., Zhang, W., Yang, X., Pootoolal, J., Chua, G., Lopez, A. *et al.* (2004) Exploration of essential gene functions via titratable promoter alleles. *Cell*, **118**, 31–44.
49. Mumberg, D., Müller, R. and Funk, M. (1995) Yeast vectors for the controlled expression of heterologous proteins in different genetic backgrounds. *Gene*, **156**, 119–122.
50. Alberti, S., Gitler, A.D. and Lindquist, S. (2007) A suite of gateway® cloning vectors for high-throughput genetic analysis in Saccharomyces cerevisiae. *Yeast*, **24**, 913–919.
51. Lousa, M., Vázquez-Huarte-Mendicoa, C., Gutiérrez, A.J., Saavedra, P., Navarro, B. and Tugores, A. (2019) Genetic epidemiology, demographic, and clinical characteristics of Charcot-Marie-Tooth disease in the island of Gran Canaria (Spain). *J. Peripher. Nerv. Syst.*, **24**, 131–138.
52. Sun, L., Song, Y., Blocquel, D., Yang, X.-L. and Schimmel, P. (2016) Two crystal structures reveal design for repurposing the C-Ala domain of human AlaRS. *Proc. Natl. Acad. Sci. U.S.A.*, **113**, 14300–14305.
53. Qin, X., Deng, X., Chen, L. and Xie, W. (2016) Crystal structure of the wild-type human GlyRS bound with tRNA(Gly) in a productive conformation. *J. Mol. Biol.*, **428**, 3603–3614.
54. Koh, C.Y., Wetzel, A.B., de van der Schueren, W.J. and Hol, W.G.J. (2014) Comparison of histidine recognition in human and trypanosomatid histidyl-tRNA synthetases. *Biochimie*, **106**, 111–120.
55. Austin, J. and First, E.A. (2002) Catalysis of tyrosyl-adenylate formation by the human tyrosyl-tRNA synthetase. *J. Biol. Chem.*, **277**, 14812–14820.
56. Yang, X.-L., Otero, F.J., Ewalt, K.L., Liu, J., Swairjo, M.A., Köhrer, C., RajBhandary, U.L., Skene, R.J., McRee, D.E. and Schimmel, P. (2006) Two conformations of a crystalline human tRNA synthetase-tRNA complex: implications for protein synthesis. *EMBO J.*, **25**, 2919–2929.
57. Raimondi, C., Brash, J.T., Fantin, A. and Ruhrberg, C. (2016) NRP1 function and targeting in neurovascular development and eye disease. *Prog. Retin. Eye Res.*, **52**, 64–83.
58. Antika, T.R., Chrestella, D.J., Ivanesthi, I.R., Rida, G.R.N., Chen, K.-Y., Liu, F.-G., Lee, Y.-C., Chen, Y.-W., Tseng, Y.-K. and Wang, C.-C. (2022) Gain of C-Ala enables AlaRS to target the L-shaped tRNAAla. *Nucleic Acids Res.*, **50**, 2190–2200.
59. Ribas de Pouplana, L., Buechter, D., Sardesai, N.Y. and Schimmel, P. (1998) Functional analysis of peptide motif for RNA microhelix binding suggests new family of RNA-binding domains. *EMBO J.*, **17**, 5449–5457.
60. Malissovas, N., Griffin, L.B., Antonellis, A. and Beis, D. (2016) Dimerization is required for GARS-mediated neurotoxicity in dominant CMT disease. *Hum. Mol. Genet.*, **25**, 1528–1542.
61. Brachmann, R.K., Vidal, M. and Boeke, J.D. (1996) Dominant-negative p53 mutations selected in yeast hit cancer hot spots. *Proc. Natl. Acad. Sci. U.S.A.*, **93**, 4091–4095.
62. Marutani, M., Tonoki, H., Tada, M., Takahashi, M., Kashiwazaki, H., Hida, Y., Hamada, J., Asaka, M. and Moriuchi, T. (1999) Dominant-negative mutations of the tumor suppressor p53 relating to early onset of glioblastoma multiforme. *Cancer Res.*, **59**, 4765–4769.
63. Quimby, B.B., Alano, A., Almashanu, S., DeSandro, A.M., Cowan, T.M. and Fridovich-Keil, J.L. (1997) Characterization of two mutations associated with epimerase-deficiency galactosemia, by use of a yeast expression system for human UDP-galactose-4-epimerase. *Am. J. Hum. Genet.*, **61**, 590–598.
64. Elsevier, J.P. and Fridovich-Keil, J.L. (1996) The Q188R mutation in human galactose-1-phosphate uridylyltransferase acts as a partial dominant negative. *J. Biol. Chem.*, **271**, 32002–32007.
65. Petropavlovskiy, A.A., Tauro, M.G., Lajoie, P. and Duennwald, M.L. (2020) A quantitative imaging-based protocol for yeast growth and survival on agar plates. *STAR Protoc.*, **1**, 100182.